# Exit channel dynamics in the ultraviolet photodissociation of the NO dimer: $(NO)_2 \rightarrow NO(A\,^2\Sigma^+) + NO(X\,^2\Pi)$

A. B. Potter, V. Dribinski, A. V. Demyanenko,[a] and H. Reisler[b]
*Department of Chemistry, University of Southern California, Los Angeles, California 90089-0482*

(Received 1 May 2003; accepted 15 July 2003)

The correlated angular and product rotational state distributions obtained in the 221.67 nm photodissociation of $(NO)_2$ yielding $NO(A\,^2\Sigma^+) + NO(X\,^2\Pi)$ have been examined in the molecular beam using the velocity map ion imaging technique. The translational energy and angular distributions of selected rotational states of $NO(A\,^2\Sigma^+)$ products in $N=0$, 5, 6 for which the maximum energies available to the $NO(X\,^2\Pi)$ products are 202.5, 142.5, and 118.5 $cm^{-1}$, respectively, have been measured. The recoil anisotropy parameter of the photofragments, $\beta_{eff}$, is $1.2\pm0.1$, less than that previously measured at 213 nm ($1.36\pm0.05$). The correlated product state distributions near dissociation threshold agree with the predictions of phase space theory. These experimental results, as well as those obtained previously at 213 nm, are compared to statistical calculations, including **v·J** correlations. Application of the $\beta$-$E_T$ correlation model to the 213 nm results indicates that $[NO(A,N), NO(X,J)]$ pairs with high $NO(X,J)$ rotational levels are produced preferentially via planar dissociation, in contrast to the statistical expectation of the **v·J** correlation, which reveals no preference for planar dissociation. A mechanism involving vibrational predissociation with restricted intramolecular vibrational energy redistribution can explain both the observed scalar and vector properties. Specifically, the low frequency torsional (out-of-plane) mode does not couple efficiently to the other modes, especially at higher excess energies when the dissociation is rapid. On the other hand, the long-range attraction between $NO(A)$ and $NO(X)$, which is revealed both in the photodissociation dynamics of the dimer and in the quenching of $NO(A)$ by $NO(X)$, encourages long-range mode couplings and can explain the largely statistical rotational state distributions observed near threshold. From images obtained near threshold, the bond energy of the NO dimer in the ground state is determined to be $710\pm10$ $cm^{-1}$, in good agreement with previous results. 
[DOI: 10.1063/1.1606442]

## I. INTRODUCTION

The nitric oxide dimer $(NO)_2$ is a weakly covalently bound complex formed by the pairing of two electrons residing originally in singly occupied $\pi^*$ orbitals of the $NO(X\,^2\Pi)$ monomers. The ground state radical has a planar *cis*-ONNO structure of $C_{2v}$ symmetry and its N–N bond length is 2.236 Å.[1] Its dissociation energy, $D_0 = 710 \pm 10\,cm^{-1}$, though low, reflects the covalent nature of the binding.[2]

This somewhat unique character of the binding raises the interesting question of which properties of the dimer reflect the chemical nature of a *cis*-ONNO molecule, and which processes exhibit behavior akin to a weakly bound complex; e.g., a van der Waals cluster. Photodissociation dynamics is particularly suitable for exploring chemical and physical properties of molecules in electronically excited states to learn about exit-channel dynamics, and the present study examines the UV photodissociation of $(NO)_2$ in the 222–213 nm region.

The electronic structure and UV photodissociation of $(NO)_2$ and its excited states have been studied before.[3–7] *Ab initio* calculations have shown the existence of a large number of electronic states that have no counterpart in the separate monomers.[8,9] States accessed in the near IR and in the UV correlate asymptotically with two $NO(X\,^2\Pi)$ radicals and with the ion pair $NO^+ + NO^-$, respectively. Between these two groups of states, lie manifolds of Rydberg and valence states that correlate asymptotically with $NO(A\,^2\Sigma^+) + NO(X\,^2\Pi)$ and $NO(B\,^2\Pi) + NO(X\,^2\Pi)$, but their energies are still unknown.[8] These two channels have been observed experimentally following photolysis at 193–210 nm,[3,5] though the mechanism and dynamics of their formation are still not well understood.

The focus of the present work is on the dynamics photoinitiated by a $^1B_2 \leftarrow {}^1A_1$ transition and terminating in the channel:

$$(NO)_2 \rightarrow NO(A\,^2\Sigma^+) + NO(X\,^2\Pi)$$
$$\Delta H = 44\,910\ cm^{-1}. \qquad \text{(I)}$$

Our goal is to determine how the products' scalar and vector properties reflect the bonding characteristics, electronic structure and the dynamics of the dissociation of the electronically excited NO dimer.

[a]Current address: Biological Imaging Center, Beckman Institute 139-74, California Institute of Technology, 1200 E. California Blvd, Pasadena, CA 91125.
[b]Electronic mail: reisler@usc.edu

 

In previous work by Kajimoto *et al.*, NO($A$) product quantum state distributions obtained via reaction I were determined following 193 nm photolysis, and could be fit by a constrained version of the statistical phase space theory (PST). In this version the fraction of products with aligned orbital angular momentum vector **L** was treated as a parameter that depended on the rotational energy of the NO products.[3,5] The NO product possessed weak alignment and vector correlations, and its recoil anisotropy parameter $\beta_{\text{eff}}$ ranged from 1.0 to 1.4 for $N=7-20$ levels of NO($A$), where $N$ is the rotational level.[10] These results, which corresponded to excess energy $E^{\dagger}=6900\,\text{cm}^{-1}$, were interpreted as an indication of fast and direct dissociation, mostly within the molecular plane. The authors concluded that the rotational axis of the NO($A$) fragment becomes more perpendicular to the dimer plane as $N$ increased.[5]

A different perspective of the dissociation was explored in the time-resolved photoelectron spectroscopy measurements carried out at 210 nm.[11] This study showed that $(\text{NO})_2$ dissociation exhibited two time scales. The initially prepared dimer state decayed in ~0.3 ps, while the NO($A$)+NO($X$) products buildup time was ~0.7 ps. It was suggested that nonadiabatic transitions might give rise to this behavior, although no definitive conclusions about the participating states could be reached.

In a recent study (Paper I),[12] we examined in detail the angular distributions obtained in the photodissociation of $(\text{NO})_2$ at 213 nm ($E^{\dagger}=2038\,\text{cm}^{-1}$) for specific NO($A$) rotational states. Using the velocity map ion imaging technique, we obtained speed-dependent recoil anisotropy parameters $\beta_{\text{eff}}$ from images of selected NO($A,N$) states. The main result was that as the c.m. translational energy, $E_{\text{T}}$, of the fragments decreased, $\beta_{\text{eff}}$ first decreased and then, at very low $E_{\text{T}}$, increased abruptly again. This $\beta$-$E_{\text{T}}$ correlation could be simulated for all the monitored NO($A,N$) states by a classical model that related the decrease in $\beta_{\text{eff}}$ at low $E_{\text{T}}$ to the deviations from axial recoil mandated by angular momentum conservation. This model, referred to in what follows as the $\beta$-$E_{\text{T}}$ correlation model, is applicable to cases where the dissociation results from an in-plane electronic transition. The model shows that for each NO($A,N$) level, high rotational states $J$ of the NO($X$) co-fragment are produced preferentially via planar dissociation, in agreement with Naitoh *et al.*,[5] and the fragments' angular momenta attain their final values at an interfragment separation of 2.6 ±0.4 Å, close to the 2.24 Å N–N equilibrium bond length in the ground state of the dimer. Except for very highly rotating NO($X,J$) states near the energetic limit, both co-rotating and counter-rotating NO products are produced.

In addition, with 213 nm photolysis both the rotational energy distributions of NO($X$) co-fragments correlated with specific NO($A,N$) states, and the global rotational state distribution of NO($A$) showed deviations from the predictions of PST. This deviation was particularly prominent for high rotational states of the NO($X$) co-fragment. It was suggested in Paper I that at $E^{\dagger}=2038\,\text{cm}^{-1}$, effects due to exit channel dynamics likely influenced both the correlated and global rotational state distributions of the NO fragments, but the deviations were small and their origin was not revealed.

In the present work, we extend our measurements to the near threshold regime ($E^{\dagger}\approx 200\,\text{cm}^{-1}$), and examine in detail both scalar and vector properties of the dissociation products. We also carry out more extensive comparisons with statistical treatments, including $\mathbf{v}\cdot\mathbf{J}$ correlations. Based on the new results, we propose a mechanism in which UV excitation accesses (directly or indirectly) a predominantly Rydberg electronic state that is weakly bound and correlates with channel I. The deviations from the statistical predictions are thought to reflect restricted IVR involving the coupling of the initial vibrational excitation to the N–N reaction coordinate. The large mismatch between the different vibrational modes renders the couplings state specific, influences the nuclear dynamics that lead eventually to product formation, and may also be reflected in the multiple dissociation time scales observed in the evolution of the excited dimer into products.[11]

## II. EXPERIMENT

The experiments are performed using $(\text{NO})_2$ generated in a seeded molecular beam of NO. The $(\text{NO})_2$ dimer is excited in a one-photon transition to above the threshold of the NO($A\,^2\Sigma^+$)+NO($X\,^2\Pi$) dissociation channel using 221.67 nm laser radiation. Following photolysis, the dimer undergoes fast dissociation, and NO($A\,^2\Sigma^+,N$) products are detected by resonance enhanced multiphoton ionization (REMPI) and velocity map ion imaging, providing velocity and angular distributions of state-selected products. The experiments are similar to those carried out at 213 nm,[12] and therefore, only procedures that have changed are discussed in detail.

Nitric oxide dimer is formed in a free jet expansion of NO in a 70% Ne: 30% He buffer. A doubly skimmed pulsed molecular beam containing 7% NO seeded in 2.0 atm of the carrier gas propagates through a hole in the repeller plate of the ion optics assembly into the ionization region. The Ne:He buffer gives better velocity resolution than pure He buffer by slowing the molecular beam and enabling the skimmers to better reduce the lateral components of the translational motion. Additionally, the greater cooling achieved in the Ne:He mixtures minimizes the contribution of parent rotational angular momentum to the overall angular momentum, which is important for near-threshold experiments, since so few rotational states of the fragments are accessible. By measuring the REMPI spectrum of the NO $A\,^2\Sigma^+\leftarrow X\,^2\Pi$ transition in mixtures of 7% NO, we estimate that the rotational temperature in the beam is $T_{\text{rot}}=2$ K with the Ne:He buffer compared with 3 K with the previously used He buffer.

Further downstream, $(\text{NO})_2$ undergoes photolysis with pulsed, linearly polarized, and mildly focused ($f.l.=50$ cm) UV laser radiation, which intersects the molecular beam at a right angle. The photolysis laser pulse is obtained by using the frequency-doubled output of an excimer laser pumped dye laser system (Coumarin 440, 0.1–0.3 mJ). The correspondence between the measured signal and $(\text{NO})_2$ photolysis has been demonstrated previously.[12]

The photolysis and probe lasers are both linearly polarized and introduced coaxially at a right angle to the molecular beam. NO($A\,^2\Sigma^+$) photofragments are probed state selec-

tively with the focused output of a Nd:YAG laser pumped dye laser system [Rhodamine 640, 0.2–0.5 mJ; $f.l.$ $=30-50$ cm lens depending on the NO($A,N$) signal] by $1+1$ REMPI via the $E\,^2\Sigma^+ \leftarrow A\,^2\Sigma^+$ transition at $\sim$600 nm.[6,13] Probing the $P$ and $R$ branches of the transition gives identical results. At the employed probe laser intensity, the monitored transitions are saturated,[14] but the results do not change when the laser intensity is reduced. To minimize complications due to vector correlations, the polarizations of the two lasers are fixed parallel to each other, and we assume that changes in the anisotropy parameter due to rotational alignment are minimal.[6] The time delay between the pump and probe lasers is kept at $0\pm5$ ns. Typical signals include the summation of $(1-2)\times10^5$ laser firings. The main source of background ion signal is non-state-selective ionization of NO($A$) fragments by the pump laser radiation. Good spatial and temporal overlap of the two laser beams minimizes the background due to ionization by the pump.

The velocity map imaging arrangement has been described in detail elsewhere.[15,16] In brief, it consists of an ion-acceleration stage, a 60 cm long drift-tube, and a CCD camera that monitors a phosphor screen coupled to a MCP ion detector. Since there is less energy available for translation of the fragments than in Paper I, the electrode voltages are reduced to expand the size of the image.

In acquiring images, the electric field vector, **E**, of the photolysis laser is maintained parallel to the vertical direction of the image plane and the product recoil velocities are aligned predominantly in the polar direction of the image. After background subtraction, the images are symmetrized and the two-dimensional (2D) projections are converted to three-dimensional (3D) velocity distributions using the Basis Set Expansion (BASEX) method.[17] This image reconstruction method is based on expanding the projection in a basis set of functions that are analytical projections of known well-behaved functions. The fragment's speed distribution is obtained at each distance from the center by analytical integration of the reconstructed image, expressed as a linear combination of basis functions, over all angles. The angular distributions are directly obtained from the expression of the image in polar coordinates.

## III. RESULTS AND ANALYSIS

Figure 1 shows representative reconstructed images of NO($A\,^2\Sigma^+,N$) fragments following 221.67 nm photolysis. The total available energy with respect to the channel I threshold is $E^\dagger=202.5\,\mathrm{cm}^{-1}$, and the maximum energies available to the NO($X$) fragments are $E_{\max}=202.5$, 142.5, and 118.5 $\mathrm{cm}^{-1}$ for $N=0$, 5, and 6, respectively. From these images we derive the binding energy of the NO dimer in its ground electronic state, $710\pm10$ $\mathrm{cm}^{-1}$, in good agreement with previous results.[2]

The speed distribution of each NO($A,N$) state is converted to a translational energy distribution $P(E_T)$ from which the correlated NO($X,\Omega,v,J$) internal energy (spin–orbit, vibrational, and rotational, respectively) distribution $P(E_{\mathrm{int}})$ is derived. Figure 2 shows the $P(E_T)$ distributions for the same NO($A,N$) states. Note that in the NO($A,N=6$) measurement ($E_{\max}=118.5\,\mathrm{cm}^{-1}$), the only spin–orbit state energetically accessible is NO($X\,^2\Pi_{1/2}$).

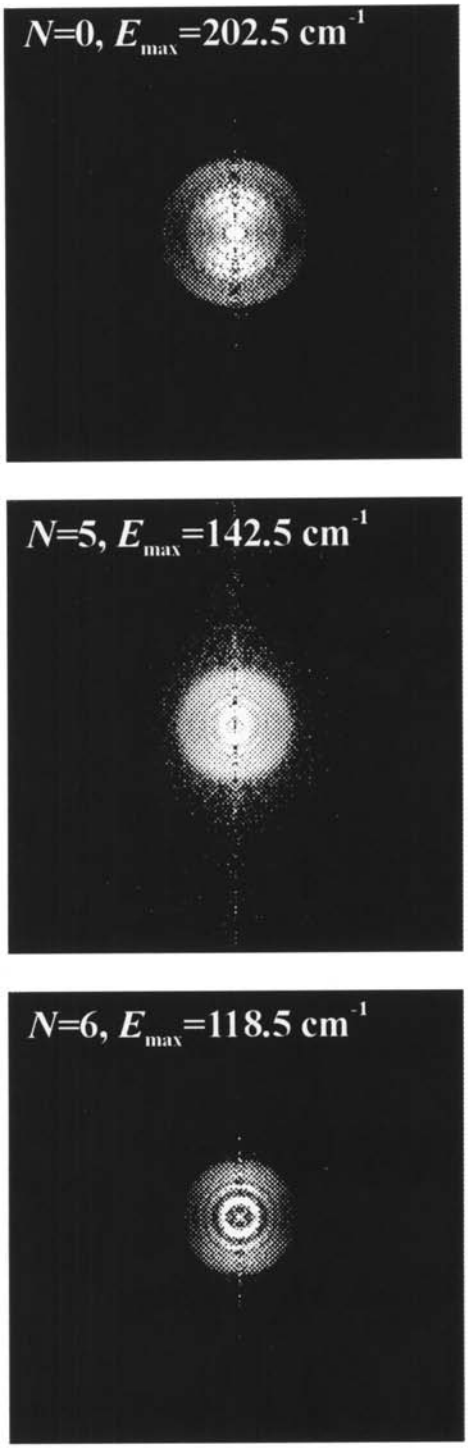


FIG. 1. 2D cuts of the reconstructed images of NO($A\,^2\Sigma^+,N=0,5,6$) obtained in photolysis of $(NO)_2$ at 221.67 nm. The maximum energies available to the NO($X$) fragment are 202.5, 142.5, and 118.5 $\mathrm{cm}^{-1}$, respectively. The electric field vector of the photolysis laser is parallel to the vertical direction of the image plane.

### A. Angular distributions

The speed-dependent recoil anisotropy parameter, $\beta_{\mathrm{eff}}(V)$, is derived from the angular distributions using[18]

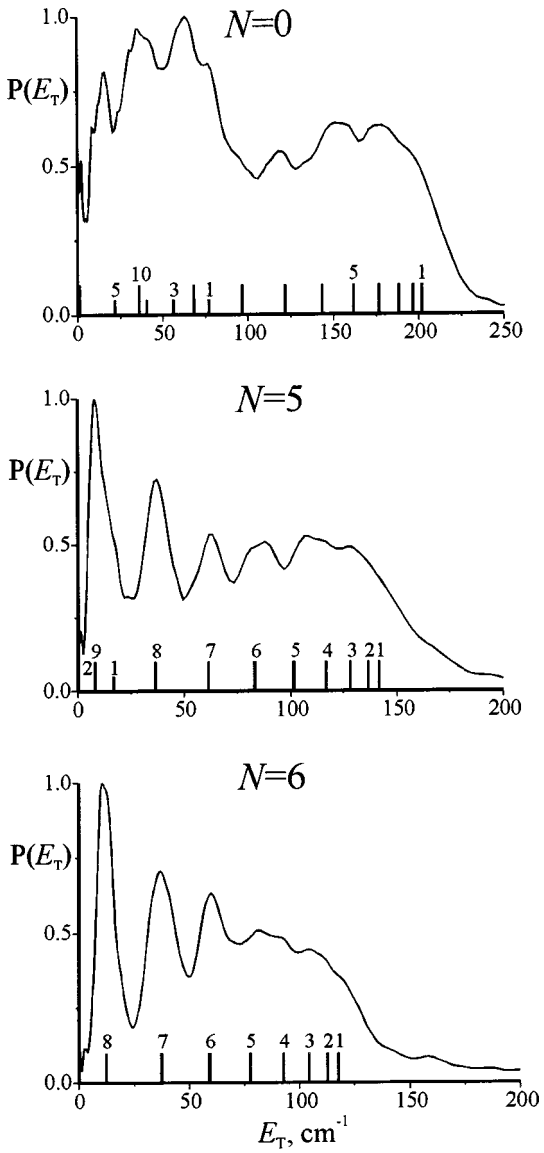


FIG. 2. Total c.m. translational energy ($E_T$) distributions of NO($A\,^2\Sigma^+, N=0,5,6$) obtained in the photodissociation of $(NO)_2$ at 221.67 nm. The vertical lines mark the rotational levels of the NO($X\,^2\Pi_{\Omega=3/2,1/2}, J$) co-fragment. The long and short lines correspond to the $\Omega=1/2$ and $\Omega=3/2$ spin–orbit states, respectively. In the $N=6$ measurement, only the NO($X\,^2\Pi_{1/2}$) spin–orbit state is accessible.

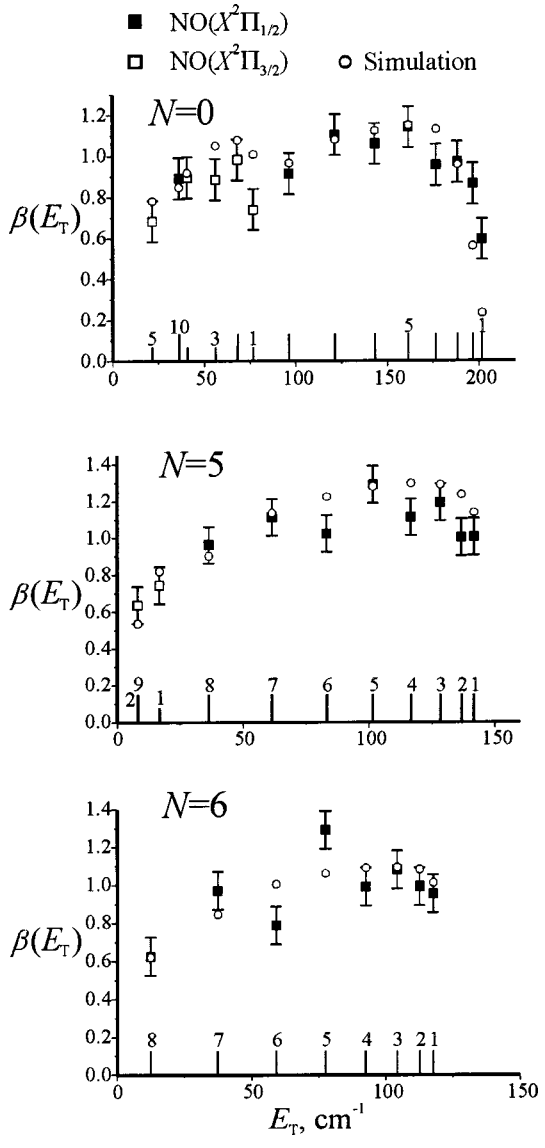


FIG. 3. Dependence of the anisotropy parameter, $\beta(E_T)$, of NO($A\,^2\Sigma^+, v=0, N=0,5,6$) on the c.m. translational energy ($E_T$) following photodissociation at 221.67 nm. The rotational level of the NO($X\,^2\Pi_{\Omega=3/2,1/2}, v=0, J$) co-fragment is specified on the vertical lines as in Fig. 2. The open and closed squares correspond to dissociation into the $\Omega=1/2$ and $\Omega=3/2$ spin–orbit states, respectively. The circles indicate the prediction of the $\beta$-$E_T$ model described in the text.

$$P(\theta,V)\propto\left(\frac{1}{4\pi}\right)[1+\beta_{\text{eff}}(V)P_2(\cos\theta)]. \quad (1)$$

$\beta_{\text{eff}}(V)$ is determined using Eq. (1) at each distance from the center of the image corresponding to an available NO($X,J$) state (i.e., a particular speed). Energy balance is given by

$$E^{\dagger}=h\upsilon-D_0=E_{\text{int}}^{\text{NO}(A)}+E_{\text{int}}^{\text{NO}(X)}+E_{\text{T}}^{\text{NO}(A)}+E_{\text{T}}^{\text{NO}(X)}, \quad (2)$$

where $D_0$ is the dissociation threshold of channel I, $E_{\text{T}}^{\text{NO}(A,X)}$ are the c.m. recoil energies of the fragments; and $E_{\text{int}}^{\text{NO}(A,X)}$ are the corresponding internal energies, (i.e., spin–orbit, vibrational, and rotational energies). Each measured $\beta_{\text{eff}}$ is a weighted average of the $\beta$ parameters associated with all the NO($X\,^2\Pi_{1/2,3/2}, J$) states whose $E_{\text{int}}$ is complementary to $E_{\text{T}}$. The solid and open squares in Fig. 3 represent measured $\beta_{\text{eff}}$ values at $E_{\text{T}}$ corresponding to the $E_{\text{int}}$ of specific NO($X\,^2\Pi_{1/2},J$) and NO($X\,^2\Pi_{3/2},J$) states, respectively. The maximum $\beta_{\text{eff}}$ value observed with $E^{\dagger}=202.5\,\text{cm}^{-1}$ is $1.2\pm0.1$, somewhat lower than the value observed at $E^{\dagger}=2038\,\text{cm}^{-1}$ ($\beta_{\text{eff}}=1.36\pm0.05$).

### B. Correlated energy distributions

The NO($X,J$) rotational state distributions correlated with specific NO($A,N$) rotational states are shown in the left hand panels of Fig. 4. To derive the correlated distributions, the fragment speed distributions were fit by a set of Gaussian functions, each centered at the position of an NO($X\,^2\Pi_{1/2,3/2},J$) state. The widths of the Gaussian functions were optimized to give the best fit for each speed distribution. The relative populations of the $J$ states were then determined by a least square fit, using Tikhonov regulariza-

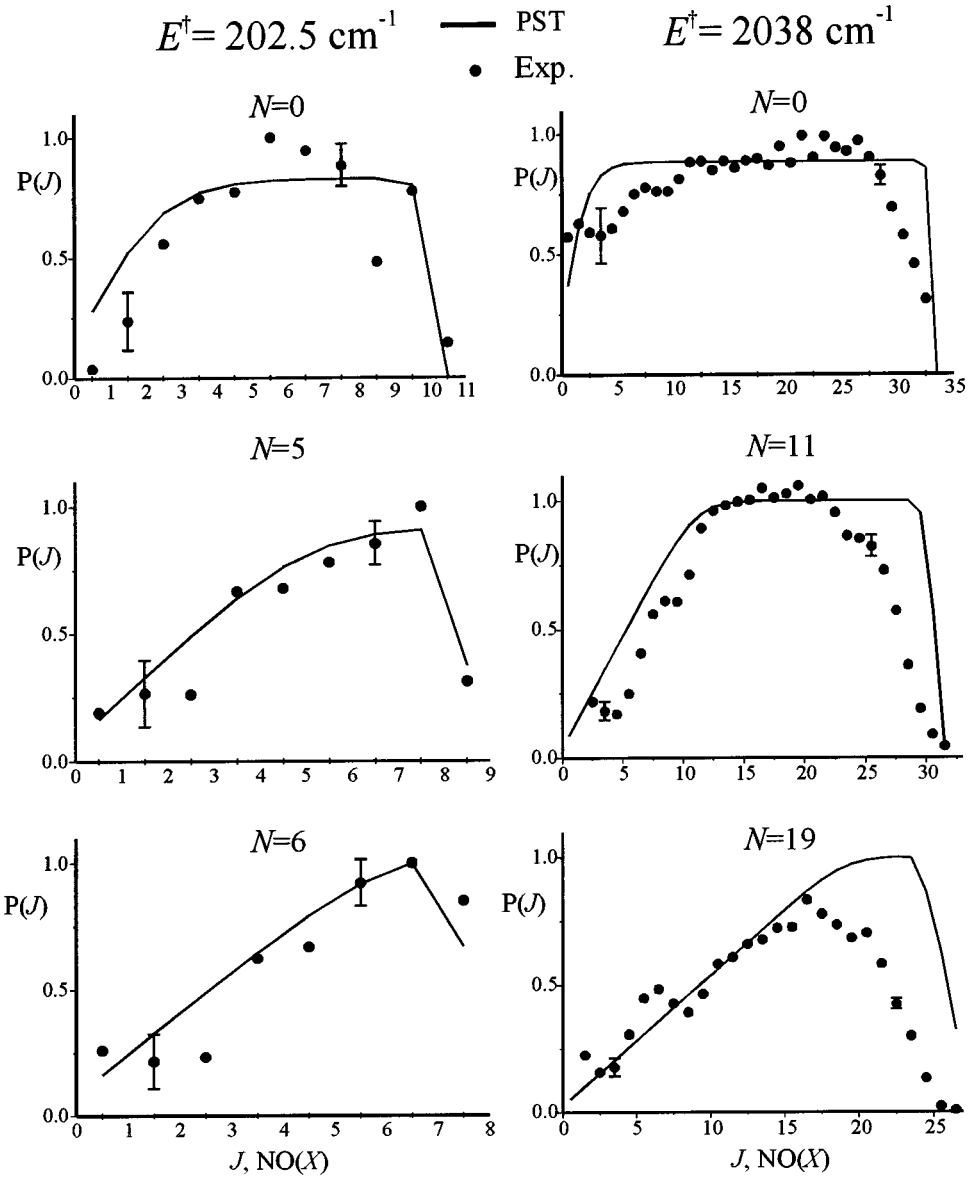


FIG. 4. Correlated distributions P($J$) of NO($X$,$J$) rotational states for specific NO($A$,$N$) states. The populations extracted from the observed translational energy distributions, P($E_T$) are indicated by circles, while the solid curve depicts the corresponding PST distribution. The left and right panels show distributions with maximum available energy of 202.5 and 2038 $cm^{-1}$, respectively.

tion to stabilize the coefficients in the overlapped region of low $J$ states.[17] The small separation between low $J$ states ($J \leqslant 3$) in the energy distribution reduces the accuracy of their extracted populations to $\pm 50\%$, while for higher $J$'s it is about $\pm 10\%$. The error is greater than in our previous $(NO)_2$ experiments at 213 nm (shown for comparison on the right-hand side of Fig. 4),[12] because of the smaller signal to noise ratio. The extracted rotational distributions in the 213 nm photolysis experiments have shown that the two spin–orbit states of NO($X$) are approximately equally populated in all the correlated distributions. Therefore, in the rotational state distributions shown in Fig. 4, the spin–orbit levels are suppressed for clarity of presentation.

## IV. DISCUSSION

### A. Scalar properties

In the PST description of bond breaking, the accessible phase space is constrained only by conservation of energy and angular momentum, which for the NO dimer distributions requires satisfying the condition set in Eq. (2) and also

$$\mathbf{J}_{(NO)_2} = \mathbf{J}_{NO(A)} + \mathbf{J}_{NO(X)} + \mathbf{L}, \tag{3}$$

where $\mathbf{J}_{(NO)_2}$, and $\mathbf{J}_{NO(A,X)}$ are the angular momenta of the parent $(NO)_2$ molecule, and the NO($A$,$X$) fragments, respectively; and $\mathbf{L}$ is the orbital angular momentum.

In our PST treatment of correlated rotational distributions in $(NO)_2$ dissociation, $N_{NO(A)}$ is selected in the experiment, the values of $J_{NO(X)}$ are determined by the available energy, and $J_{(NO)_2}$ is determined by the rotational temperature of the parent in the molecular beam ($T_{rot} = 2$ K).[10] The $L$ states are counted for each specific $J_{NO(A)}$, $J_{NO(X)}$, and $J_{(NO)_2}$ combination allowed by the conservation of energy and angular momentum, and the result for each $J_{(NO)_2}$ is weighted according to a 2 K Boltzmann distribution.

The correlated rotational state distributions obtained at 221.67 nm ($E^\dagger = 202.5\ cm^{-1}$) agree well with the statistical predictions shown in solid lines in Fig. 4. However, at the

higher available energy ($E^{\dagger}=2038\,\mathrm{cm}^{-1}$), both the correlated rotational distribution and the global NO($A$) rotational state distributions are overestimated by PST for high $J$ states (see Fig. 4 and Paper I).[12] These deviations from PST predictions are fairly small but consistent, and from scalar properties alone we cannot elucidate their nature.

### B. Vector properties

In previous papers,[12,19] the $\beta$-$E_T$ correlation model, a classical model based on energy and angular momentum conservation, was used to explain the measured dependence of the recoil anisotropy parameter $\beta_{\mathrm{eff}}$ on the translational energy of the recoiling fragments in the photodissociation of tri-atomic[19] and tetra-atomic[12] species. In applying the model, a critical distance $R_C$ where the rotational and orbital angular momenta were established was inferred from fits to the data. For the NO dimer, $R_C$ was defined as the distance between the centers-of-mass of the two NO fragments,[12] and it was, therefore, loosely related to the value of $R$ at the transition state ($R_C \geqslant R_{TS}$). In simulating the dependence of $\beta_{\mathrm{eff}}$ on $E_T$, we examined two models, one in which the dissociation was constrained to the plane, and one in which a constraint was not imposed. Based on comparisons with the experimental $\beta_{\mathrm{eff}}$ versus $E_T$ curves, we concluded that in 213 nm photolysis, dissociation into high rotational levels of NO($X$) must take place from a planar $(NO)_2$ geometry and the best fit was obtained for $R_C=2.6\pm0.4$ Å. We assume that both co-rotating and counter-rotating NO fragments are produced, except for the highest allowed $J$ states, for which only counter-rotating fragments satisfy both energy and angular momentum conservation.[12]

The results of the $\beta$-$E_T$ correlation model obtained for 221.67 nm photolysis are depicted by circles in Fig. 3. The best fits are obtained for $R_C=3.0\pm0.4$ Å, and the planar and unconstrained dissociation models fit the data equally well. Evidently, in this case the model cannot serve to identify a geometrical bias in the dissociation.

The $\beta$-$E_T$ correlation model indicates that at $E^{\dagger}=2038\,\mathrm{cm}^{-1}$, dissociation into high NO($X,J$) states preferentially takes place in the NO dimer plane. In addition, comparisons with PST calculations show that the populations of these high NO($X,J$) fragments deviate from statistical predictions. It remains unclear, though, whether the deviation from the statistical prediction of the rotational state distribution is associated with the requirement for planar dissociation derived from the $\beta$-$E_T$ correlation model. Planarity implies that the NO velocity vector **v**, which lies in the plane, must be perpendicular to **J**, and the question arises whether a perpendicular **v**·**J** correlation for high $J$ states is required by statistical theories. For example, in dissociation of a nonrotating NO dimer into one nonrotating and one rotating fragment (the pseudo-triatomic case), the rotational angular momentum of the *rotating* fragment has to be balanced mainly by **L**, causing **v** to be perpendicular to **J**. In such a case, the statistical prediction would indicate planar dissociation.

In order to determine if this is the case here, the statistical prediction of the **v**·**J** vector correlation has been calculated. While the traditional PST calculation described above

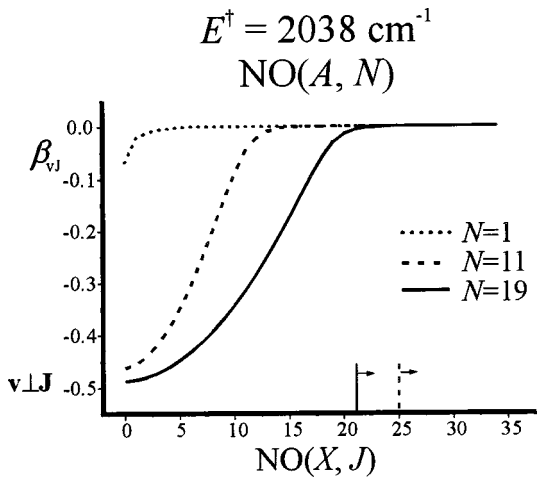


FIG. 5. PST prediction of the **v**·**J** correlation in the 213 nm ($E^{\dagger}=2038\,\mathrm{cm}^{-1}$) photodissociation of $(NO)_2$ for selected [NO($A,N$), NO($X,J$)] pairs. The dotted, dashed, and solid lines represent dissociation into $N=1$, 11, and 19, respectively. The solid and dashed vertical lines represent the lowest NO($X$) co-fragment $J$ level for which planar dissociation (**v** perpendicular to **J**; $\beta_{vJ}=-1/2$) was inferred from the experiments for pairs with $N=11$ and 19, respectively. This is in contrast to the statistical **v**·**J** calculation, which predicts no such correlation.

is convenient for calculating scalar product state distributions, it is not as well suited to describe **v**·**J** correlations. These are more easily calculated by using the helicity state count for PST developed by North and Hall.[20] An advantage of their method is that in the helicity basis, the projections of the fragments angular momenta on the recoil axis are good quantum numbers, while the orbital angular momentum **L** has no projection on this axis.

To perform the helicity state count for the **v**·**J** correlation (without including a centrifugal barrier), the angular momenta of the individual fragments $\mathbf{J}_i$ are described by their projections on the center-of-mass relative velocity vector, $\lambda_i=-J_i\cdots J_i\,[i=\mathrm{NO}(A),\mathrm{NO}(X)]$. The total helicity, $\Lambda=\lambda_{\mathrm{NO}(A)}-\lambda_{\mathrm{NO}(X)}$, is contstrained by $J_{(NO)_2}$ due to angular momentum conservation such that $|\Lambda|\leqslant J_{(NO)_2}$. The statistical prediction of the $\mathbf{v}\cdot\mathbf{J}_{\mathrm{NO}(A)}$ correlation for dissociation into a given $(J_{\mathrm{NO}(A)},J_{\mathrm{NO}(X)})$ pair is given by the second Legendre moment of the normalized $p(\lambda_{\mathrm{NO}(A)})$ distribution[20]

$$\beta_{vJ,J_{\mathrm{NO}(A)},J_{\mathrm{NO}(X)}}=\sum_{\lambda_{\mathrm{NO}(A)}=-J_{\mathrm{NO}(A)}}^{J_{\mathrm{NO}(A)}} p(\lambda_{\mathrm{NO}(A)})_{J_{\mathrm{NO}(X)}} \times P_2\left(\frac{\lambda_{\mathrm{NO}(A)}}{\sqrt{J_{\mathrm{NO}(A)}(J_{\mathrm{NO}(A)}+1)}}\right), \qquad (4)$$

where $\beta_{vJ}$ is the bipolar moment corresponding to the **v**·**J** correlation [denoted elsewhere by $\beta_0^0(22)$].[21] The limiting values of $\beta_{vJ}$ are $-1/2$ and 1, corresponding to **v** perpendicular and parallel to **J**, respectively.[22] The results of the statistical calculations of $\beta_{vJ}$ for NO($A,N=1,11,19$) paired with the allowed NO($X,J$) states are shown in Fig. 5 for dissociation at 213 nm and $T_{\mathrm{rot}}=3$ K (the rotational temperature of the NO dimer in the 213 nm experiments).[12]

For NO($A,N$) pairs associated with the $J=0$ state of NO($X$), a perpendicular **v**·**J** correlation similar to that of a triatomic molecule should be obtained. However, even in this

case $\beta_{vJ}$ can deviate from its limiting $-1/2$ value, because some of the orbital angular momentum can be compensated by parent molecule rotation, resulting in less negative values of $\beta_{vJ}$. The effect of parent rotation diminishes as $N$ increases, because fewer of the allowed $L$ states are balanced by $\mathbf{J}_{(NO)_2}$. Similarly, the deviations from the $-1/2$ limit increase at higher $T_{rot}$.

In general, when both fragments in an $[NO(A,N),NO(X,J)]$ pair have low rotational angular momenta, the parent rotational angular momentum makes a significant contribution, causing the **v·J** correlation to be small. When both have higher (but comparable) rotational angular momenta, the fragments can balance each other's angular momenta by counter-rotating, and again the **v·J** correlation is small. For example, when $N \approx J$ the predicted value is $\beta_{vJ} \approx 0$. The **v·J** correlation calculations predict that in general when monitoring an intermediate $NO(A,N)$ level such as $N=11$ or 19 ($J_{max}=34$), there will be a perpendicular **v·J** correlation with associated low $NO(X,J)$ levels, but *not* with high $J$ levels. This is clearly seen in Fig. 5. Although a centrifugal barrier is not included in this calculation, its effect is small and does not change the qualitative prediction. Its inclusion would drive the $\beta_{vJ}$ value of the highest $NO(X,J)$ states to slightly more *positive* values corresponding to a decreased correlation. This has been described in detail elsewhere.[20]

From our perspective, the main conclusion to be drawn from the **v·J** correlation calculations is that for all the $NO(A,N)$ states investigated in our work, the statistical calculations do not predict a perpendicular **v·J** correlation. Thus, the statistical prediction does not dictate the planar dissociation inferred from the experiments of Paper I for high $NO(X,J)$ states. Again, it is important to emphasize that when applying the $\beta$-$E_T$ correlation model to the dissociation of $(NO)_2$ we have not assumed *a priori* that there is a preference for planar dissociation. The conclusion that planarity is the preferred geometry for high $J_{NO(X)}$ pairs is based on the fit of the curve of $\beta_{eff}$ versus $E_T$ to the data.[12] Therefore, the discrepancy between the experimental findings and the statistical predictions for both scalar and vector properties for pairs with high $NO(X,J)$ states indicates that nonstatistical effects are important in the product state distributions obtained in the UV dissociation of the NO dimer.

### C. Dissociation mechanism

Electronic structure considerations and experiments indicate that the transition dipole moment of the $(NO)_2$ $^1B_2 \leftarrow {}^1A_1$ system lies in the molecular plane, parallel to the N–N bond.[5–7] This geometry corresponds to the limiting value $\beta=2$. As discussed in Paper I, the observed reduction of the measured $\beta_{eff}$ from its limiting value is partly due to dissociation lifetime, which is close to a picosecond at 210 nm.[11] Additional reduction in $\beta$ may be due to out-of-plane motions and rotation of the recoil axis with change in the molecular geometry during dissociation. Our measurements at 213.00, 216.00, and 221.67 nm yield maximum $\beta_{eff}$ values of $1.36 \pm 0.05$, $1.30 \pm 0.05$, and $1.2 \pm 0.1$, respectively, suggesting that the lifetime increases as the available energy decreases.

An important requirement for statistical dissociation is that the internal energy of the parent molecule is redistributed randomly among its vibrational modes on a time scale faster than bond breaking. At energies close to the dissociation threshold, the parent lifetime is longer, allowing more time for the $(NO)_2$ internal energy to be randomized prior to dissociation. At higher $E^\dagger$ the dissociation may be too fast for all the modes to be populated, explaining why the correlated product state distributions at $E^\dagger = 2038\ cm^{-1}$ appear less statistical than at $E^\dagger = 202.5\ cm^{-1}$.

With respect to intramolecular vibrational energy redistribution (IVR), the dissociation of the NO dimer on the excited state resembles vibrational predissociation of a van der Waals complex.[23] In both species the frequencies of the intermolecular dimer modes are much lower than the frequencies of the vibrational modes of the individual sub-units. The large disparity between these frequencies leads to small coupling matrix elements between the molecular modes of the sub-units and the intermolecular modes, resulting in restricted IVR.

The preference for planarity for the high $NO(X,J)$ co-fragments suggests a restricted involvement of the torsional (out-of-plane) mode in the excited NO dimer. The reduced participation of the torsional mode can be explained by the following argument. If we assume that the initial excitation involves the NO moiety,[8,24] i.e., excitation of the NO stretch, then for dissociation to occur, energy must flow into the N–N bond. Assuming further that the vibrational frequencies in the excited state are similar to those in the ground state neutral and cation (which are comparable), we can use $\sim 1800$, $\sim 300$, $\sim 200$, and $\sim 100\ cm^{-1}$ for the NO stretch, NNO bend, NN stretch, and torsion, respectively.[25] Consequently, couplings are expected to be weak between the NO stretch and all the other modes, strong between the NNO bend and the NN stretch, and weakest to the torsion. It is reasonable then that the high levels of the torsional modes, which give rise to out-of-plane dissociation, are not efficiently excited, in particular at high excess energies.

### D. The nature of the dissociative state

We have argued above that the decreased propensity for out-of-plane dissociation for NO products in high $J$ states can reflect small coupling matrix elements to the low-frequency torsional mode of the excited state. This excited state, however, remains unassigned. Though we limited our measurements to wavelengths where channel I predominates, it should be remembered that more than one electronic state of the dimer can give rise to this channel. Moreover, *ab initio* calculations show that in the 1 eV energy range around the threshold of channel I (i.e., $\sim 50\,000 \pm 5000\ cm^{-1}$), there are 4 singlet Rydberg states and 8 singlet valence states.[8] The group of 4 ion-pair states is not much higher in energy.[8] It is quite plausible, therefore, that the adiabatic electronic states include contributions from several diabatic states, and that the mixing among states varies along the N–N reaction coordinate. This has been seen in other dissociating molecules

and radicals that have valence and Rydberg states in close proximity.[26,27] In our case, the initially excited state may possess, for example, a large ns or $np_{x,y,z}$ Rydberg character mixed with valence states that correlate asymptotically with the $NO(B\,^2\Pi)+NO(X\,^2\Sigma)$ channel (whose threshold is only 1280 $cm^{-1}$ above channel I), and/or ion-pair states. This scenario does not exclude, of course, nonadiabatic transitions.

If indeed the dissociative state has a predominantly Rydberg character, its N–N bonding is probably intermediate between that of the neutral and ionic ground states, which are bound by ~700 and ~5000 $cm^{-1}$, respectively.[32] By using 1+1 ionization of jet-cooled $(NO)_2$, we found that UV absorption commences at $41\,500\pm200$ $cm^{-1}$.[31] If dissociation to channel I takes place on the initially excited state, this state would be bound by $3400\pm200$ $cm^{-1}$. Such a shallow well in the N–N coordinate would explain the incomplete IVR in the dissociation, which would become more severe when (i) the dissociation is faster; and (ii) higher excitation of the torsional mode is required.

Alternatively, one can look at the inverse process to dissociation, i.e., the association of NO($X$) and NO($A$), and gain insight by considering what is known about the quenching of NO($A$) in collisions with NO($X$), a process which has been studied extensively.[28] The efficient quenching has been attributed, at least in part, to strong electrostatic interactions between NO($A$) and NO($X$), which are enhanced by the large dipole moment of NO($A$) (1.1 D).[29] These attractive interactions extend to long range, rationalizing the $R_C$ value of ~3.0 Å obtained in the near threshold photodissociation experiments. This also helps explain the statistical behavior observed near the threshold of reaction I. At shorter N–N distances, the electrostatic attraction switches to a bonding valence interaction.

Blanchet and Stolow, who carried out femtosecond photoelectron spectroscopy experiments at 210 nm, inferred that a nonadiabatic decay pathway may be involved in the dissociation.[11] This explained the faster disappearance of the parent ion signal compared to the buildup of the photoelectron spectrum of the NO($A$) product. However, femtosecond absorption can coherently excite a superposition of states, which then dephases (e.g., *s* and *p* Rydberg states, or a Rydberg and a valence state). In this regard, the first excitation step in the femtosecond and nanosecond experiments may be different.

Last, we wish to comment on the issue of molecular (*cis*-ONNO) versus complex ($(NO)_2$) properties of the NO dimer. There are similarities between our proposed dissociation mechanism of the NO dimer and that of nitrite molecules (RO–NO). In the dissociation of $CH_3ONO(S_1)$ into $CH_3O+NO$, for example, excitation is initially localized in the NO moiety, and there is a shallow well along the –O–NO coordinate. Because of the weak coupling between the initially excited mode and the dissociation mode, the lifetime is long enough to allow oscillation in the $CH_3ON$–O coordinate before sufficient energy accumulates in the $CH_3O$–NO coordinate for dissociation to occur.[23] Restricted IVR is illustrated also in molecules with low dissociation thresholds and high frequency vibrational modes, such as the HOCl ground-state dissociation into HO+Cl following OH overtone excitation.[30]

## V. SUMMARY AND CONCLUSIONS

The UV photodissociation of the NO dimer has been studied at the pair correlation level with emphasis on the dynamics of the NO($X$)+NO($A$) channel. Both vector and scalar properties have been examined from 221 nm ($E^\dagger=202$ $cm^{-1}$) to 213 nm ($E^\dagger=2038$ $cm^{-1}$). The major findings from this work, as well as from Paper I are summarized below:

(1) At the higher excess energy, both the global NO($A$) distribution, and the correlated distributions display deviations from the predictions of PST, especially for high NO($X,J$) rotational levels. Near threshold, the deviations are insignificant.

(2) The maximum value of $\beta_{\text{eff}}$ at each excess energy, obtained from the measured angular distributions as a function of $E_T$, is typical of fast dissociation following a parallel transition, but is lower than the limiting value of 2.0. $\beta_{\text{eff}}$ decreases with decreasing excess energy, and part of this reduction is due to increased dissociation lifetime. This is confirmed in the time-resolved measurements of Blanchet and Stolow,[11] which show a buildup time of ~1 ps for the NO($A$) product.

(3) The $\beta$-$E_T$ correlation model indicates that for [NO($A,N$),NO($X,J$)] pairs with high NO($X,J$) rotational levels planar dissociation is favored, at least at high $E^\dagger$. This result is in agreement with the findings of Naitoh *et al.* at 193 nm.[5] This propensity for planarity, which corresponds to **v** perpendicular to **J**, is compared with statistical calculations of the **v**·**J** correlation. It is concluded that statistical considerations cannot rationalize the observed preference for planar dissociation for the high NO($X,J$) states.

A mechanism involving vibrational predissociation with restricted IVR is proposed to explain the observed scalar and vector properties. Specifically, the low frequency torsional (out-of-plane) mode does not couple efficiently to the other modes, especially at higher excess energies when the dissociation is fast. On the other hand, the long-range attraction between NO($A$) and NO($X$), which is revealed both in the photodissociation dynamics of the dimer and in the quenching of NO($A$) by NO($X$), encourages IVR and can explain the more statistical rotational state distributions observed near the threshold.

Open questions still remain regarding the nature of the initially excited state and the role of nonadiabatic transitions. Our preliminary results on REMPI of the NO dimer in the molecular beam place the threshold of the UV absorption at $41\,500\pm200$ $cm^{-1}$, but do not reveal how many states are involved in the dissociation. If dissociation to channel I takes place directly on the initially excited state, this state would be bound by $3400\pm200$ $cm^{-1}$. This binding strength is intermediate between the ground states of the neutral (~700 $cm^{-1}$) and the ion (~5000 $cm^{-1}$), suggesting a large Rydberg character for the excited state. Experiments are in progress in our laboratory to further characterize the excited state(s).

## ACKNOWLEDGMENTS

Support by the National Science Foundation and the Donors of the Petroleum Research Fund, administered by the American Chemical Society is gratefully acknowledged. We thank Albert Stolow and Carl Hayden for helpful discussions and sharing with us unpublished results on coincidence photoelectron–photofragment measurements of NO dimer dissociation.

[1] S. G. Kukolich, J. Mol. Spectrosc. **98**, 80 (1983); A. R. W. McKellar, J. K. G. Watson, and B. J. Howard, Mol. Phys. **86**, 273 (1995); S. G. Kukolich and S. M. Sickafoose, *ibid.* **89**, 1659 (1996).
[2] J. R. Hetzler, M. P. Casassa, and D. S. King, J. Phys. Chem. **95**, 8086 (1991); E. A. Wade, J. I. Cline, K. T. Lorenz, C. Hayden, and D. W. Chandler, J. Chem. Phys. **116**, 4755 (2002).
[3] O. Kajimoto, Prog. Theor. Phys. Suppl. **116**, 167 (1994).
[4] O. Kajimoto, K. Honma, and T. Kobayashi, J. Phys. Chem. **89**, 2725 (1985); H. J. Bernstein and G. Herzberg, J. Chem. Phys. **15**, 77 (1947); J. Billingsley and A. B. Callear, Trans. Faraday Soc. **67**, 589 (1971).
[5] Y. Naitoh, Y. Fujimura, F. Honma, and O. Kajimoto, J. Phys. Chem. **99**, 13652 (1995).
[6] Y. Naitoh, Y. Fujimura, K. Honma, and O. Kajimoto, Chem. Phys. Lett. **205**, 423 (1993).
[7] Y. Naitoh, Y. Fujimura, O. Kajimoto, and K. Honma, Chem. Phys. Lett. **190**, 135 (1992).
[8] A. L. L. East, J. Chem. Phys. **109**, 2185 (1998).
[9] R. Sayos, R. Valero, J. M. Anglada, and M. Gonzalez, J. Chem. Phys. **112**, 6608 (2000).
[10] Since NO($A$) belongs to Hund's case (b), the rotational energy is best described by the quantum number $N$. Consequently, the specific NO($A\,^2\Sigma^+, N$) state chosen in the experiment corresponds to two different $J$ levels ($J = N \pm 1/2$).
[11] V. Blanchet and A. Stolow, J. Chem. Phys. **108**, 4371 (1998).
[12] A. V. Demyanenko, A. B. Potter, V. Dribinski, and H. Reisler, J. Chem. Phys. **117**, 2568 (2002).
[13] M. W. Feast, Can. J. Res., Sect. A **28**, 488 (1950); K. P. Huber and G. Herzberg, *Molecular Spectra and Molecular Structure, Constants of Diatomic Molecules, Vol. VI* (Van Nostrand Reinhold, New York, 1979); G. Meijer, M. Ebben, and J. J. Termeulen, Chem. Phys. **127**, 173 (1988); A. Timmermann and R. Wallenstein, Opt. Commun. **39**, 239 (1981).
[14] M. N. R. Ashfold, R. N. Dixon, J. D. Prince, B. Tutcher, and C. M. Western, J. Chem. Soc., Faraday Trans. 2 **82**, 1257 (1986).
[15] A. Sanov, T. Droz-Georget, M. Zyrianov, and H. Reisler, J. Chem. Phys. **106**, 7013 (1997).
[16] D. H. Parker and A. Eppink, J. Chem. Phys. **107**, 2357 (1997); A. Eppink and D. H. Parker, Rev. Sci. Instrum. **68**, 3477 (1997).
[17] V. Dribinski, A. Ossadtchi, V. A. Mandelshtam, and H. Reisler, Rev. Sci. Instrum. **73**, 2634 (2002).
[18] R. N. Zare and D. R. Herschbach, Proc. IEEE **51**, 173 (1963).
[19] A. V. Demyanenko, V. Dribinski, H. Reisler, H. Meyer, and C. X. W. Qian, J. Chem. Phys. **111**, 7383 (1999).
[20] S. W. North and G. E. Hall, J. Chem. Phys. **104**, 1864 (1996).
[21] R. N. Dixon, J. Chem. Phys. **85**, 1866 (1986).
[22] For the purposes of the statistical **v**·**J** correlation calculation, the distinction between $J$ and $N$ is neglected.
[23] R. Schinke, *Photodissociation Dynamics* (Cambridge University Press, Cambridge, 1993).
[24] J. Mason, J. Chem. Soc. Dalton Trans. **1975**, 19.
[25] A. L. L. East and J. K. G. Watson, J. Chem. Phys. **110**, 6099 (1999); B. Urban, A. Strobel, and V. E. Bondybey, *ibid.* **111**, 8939 (1999).
[26] S. V. Levchenko, A. V. Demyanenko, V. L. Dribinski, A. B. Potter, H. Reisler, and A. I. Krylov, J. Chem. Phys. **118**, 9233 (2003); S. V. Levchenko and A. I. Krylov, J. Chem. Phys. **115**, 7485 (2001).
[27] C. Sandofry, Top. Curr. Chem. **86**, 91 (1979).
[28] P. H. Paul, J. A. Gray, J. L. Durant, and J. W. Thoman, Jr., Chem. Phys. Lett. **259**, 508 (1996); G. D. Greenblatt and A. R. Ravishankara, *ibid.* **136**, 501 (1987); Y. Haas and G. D. Greenblatt, J. Phys. Chem. **90**, 513 (1986); R. Zhang and D. R. Crosley, J. Chem. Phys. **102**, 7418 (1995).
[29] J. A. Gray, R. L. Farrow, J. L. Durant, and T. R. Thorne, J. Chem. Phys. **99**, 4327 (1993).
[30] A. Calegari and T. R. Rizzo, Chem. Soc. Rev. **30**, 214 (2001); A. Calegari, J. Rebstein, J. S. Muenter, R. Jost, and T. R. Rizzo, J. Chem. Phys. **111**, 123 (1999).
[31] V. Dribinski, A. B. Potter, and H. Reisler (unpublished).
[32] I. Fischer, A. Strobel, J. Staecker, G. Niedner-Schatteburg, and V. E. Bondybey, J. Chem. Phys. **96**, 7171 (1992).